THE JOURNAL OF BIOLOGICAL CHEMISTRY VOL. 286, NO. 10, pp. 7975–7982, March 11, 2011

Sugar Binding Residue Affects Apparent Na^+ Affinity and Transport Stoichiometry in Mouse Sodium/Glucose Cotransporter Type 3B*

Received for publication, October 8, 2010, and in revised form, December 20, 2010 Published, JBC Papers in Press, December 27, 2010, DOI 10.1074/jbc.M110.187880

Ana Díez-Sampedro[1] **and Stephanie Barcelona**

From the Department of Physiology and Biophysics, Miller School of Medicine, University of Miami, Miami, Florida

SGLT1 is a sodium/glucose cotransporter that moves two Na^+ ions with each glucose molecule per cycle. SGLT3 proteins belong to the same family and are described as glucose sensors rather than glucose transporters. Thus, human SGLT3 (hSGLT3) does not transport sugar, but extracellular glucose depolarizes the cell in which it is expressed. Mouse SGLT3b (mSGLT3b), although it transports sugar, has low apparent sugar affinity and partially uncoupled stoichiometry compared with SGLT1, suggesting that mSGLT3b is also a sugar sensor. The crystal structure of the *Vibrio parahaemolyticus* SGLT showed that residue Gln^{428} interacts directly with the sugar. The corresponding amino acid in mammalian proteins, 457, is conserved in all SGLT1 proteins as glutamine. In SGLT3 proteins, glutamate is the most common residue at this position, although it is a glycine in mSGLT3b and a serine in rat SGLT3b. To test the contribution of this residue to the function of SGLT3 proteins, we constructed SGLT3b mutants that recapitulate residue 457 in SGLT1 and hSGLT3, glutamine and glutamate, respectively. The presence of glutamine at residue 457 increased the apparent Na^+ and sugar affinities, whereas glutamate decreased the apparent Na^+ affinity. Moreover, glutamate transported more cations per sugar molecule than the wild type protein. We propose a model where cations are released intracellularly without the release of sugar from an intermediate state. This model explains the uncoupled charge:sugar transport phenotype observed in wild type and G457E-mSGLT3b compared with SGLT1 and the sugar-activated cation transport without sugar transport that occurs in hSGLT3.

Members of the SLC5 cotransporter family present highly diverse functions. They are capable of cotransporting Na^+ with glucose (SGLT1 and SGLT2), with myoinositol (SMIT), with iodide (NIS), or with choline (CHT), among other substrates (reviewed in Ref. 1). In fact, there is one family member, human SGLT3, that is not a transporter but is a glucose sensor (2, 3).

The crystal structures of Na^+ symporters from different families reveal that they share a core of 10 transmembrane segments composed of an inverted repeat of five segments (4). The crystal structure of *Vibrio parahaemolyticus* SGLT (vSGLT)[2] clearly resolved the residues of the sugar binding site (5). One residue that directly interacts with the sugar is glutamine 428, which is equivalent to amino acid 457 in mammalian SGLT proteins. Notably, the identity of the amino acid at position 457 in human SGLT1 (hSGLT1) has proven to have a dramatic effect on the function of the protein. Structure-function studies on hSGLT1 suggest that residue 457 interacts with sugar (6), and mutations of this residue cause glucose-galactose malabsorption (7, 8).

The crystal structure of vSGLT did not reveal the position of the single Na^+-binding site. SGLT1 and other transporters like LeuT, and presumably SGLT3, have two Na^+-binding sites. Based on structural homology to LeuT, whose two Na^+-binding sites were identified, Na1 and Na2 (9), a Na^+-binding site in vSGLT ~ 10 Å away from the sugar binding site was proposed and corresponds to Na2 in LeuT (5). The location of the other Na^+ binding site in SGLT has not been identified, but it may correspond to Na1 in LeuT. These Na^+-binding sites are likely to be conserved in SGLT1 and SGLT3 proteins.

Despite ~70% amino acid identity between hSGLT3 and hSGLT1, there are significant differences in their function, besides the inability of hSGLT3 to transport sugar. hSGLT3 also has a weaker apparent glucose affinity, no visible pre-steady-state currents and a different tissue distribution than SGLT1 (2, 10). In terms of amino acid sequence, all SGLT1 and SGLT2 proteins have a glutamine at residue 457, whereas most SGLT3 proteins have a glutamate. There are two exceptions, glycine in mouse SGLT3b and serine in rat SGLT3b (Fig. 1).

Because of the strict conservation of amino acid 457 among the SGLT1 and SGLT2 glucose transporters and the difference with the SGLT3 glucose sensors, we explored whether the identity of this residue plays a major role in the differences in function between the different proteins. Specifically, we looked at the effect of modifying this residue in mSGLT3b. We sought to learn whether the identity of residue 457 in mSGLT3b would lead to significant changes in function. We made two mutations, G457Q-mSGLT3b and G457E-mSGLT3b, to recapitulate the residue in SGLT1 and human SGLT3, respectively. We then compared the characteristics of each of the mutants with the wild type protein.

* This work was supported by the Florida Biomedical Research Program (to A. D.-S.).

[1] To whom correspondence should be addressed: Rm. 4054, Rosenstiel Bldg., Dept. of Physiology and Biophysics, Miller School of Medicine, University of Miami, 1600 NW 10th Ave., Miami, FL 33136. Tel.: 305-243-6670; Fax: 305-243-5931; E-mail: adiezsampedro@med.miami.edu.

[2] The abbreviations used are: vSGLT, *V. parahaemolyticus* SGLT; SGLT, sodium/glucose transporter; αM-Glc, α-methylglucose; hSGLT3, human SGLT3; mSGLT3b, mouse SGLT3b; 6DO-Glc, 6-deoxyglucose.

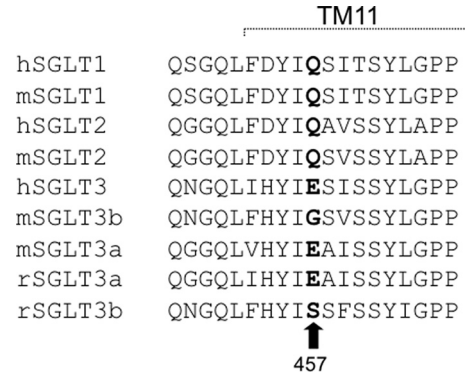

FIGURE 1. **Amino acid alignment of several SGLT proteins.** All the SGLT1 and SGLT2 proteins present a glutamine at position 457, whereas the residue at this position in SGLT3s are glutamate, glycine, or serine. *h*, human; *m*, mouse; *r*, rat; *TM11*, transmembrane segment 11.

We found that the mutations changed the apparent affinity for sugar, as expected for being part of the sugar binding site, and surprisingly, also changed the apparent affinity of Na^+. In addition, we found that residue 457 affects the charge:sugar cotransport ratio, indicating that it contributes to the uncoupled phenotype that occurs in SGLT3. We propose a mechanism for SGLT that explains the uncoupled transport that occurs in wild type mSGLT3b, G457E, and also in human SGLT3.

EXPERIMENTAL PROCEDURES

Mutagenesis—Mouse SGLT3b cDNA in pGH19 was used as a template for site-directed mutagenesis using a QuikChange kit (Stratagene). The oligonucleotide primers used were as follows: G457E-mSGLT3b (G457E-sense, 5′-CTCTTCCACTATATTGAGTCAGTTTCTAGCTAC-3′ and G457E -antisense, 5′-GTAGCTAGAAACTGACTCAATATAGTGGAAGAG-3′) and G457Q-mSGLT3b (G457Q-sense, 5′-CTCTTCCACTATATTCAGTCAGTTTCTAGCTAC-3′ and G457Q-antisense, 5′-GTAGCTAGAAACTGACTGAATATAGTGGAAGAG-3′. The underlined letters represent the nucleotides changed. The gene was sequenced from start to stop codon to ensure that only the desired mutation was present.

Expression of Proteins in Xenopus laevis Oocytes—Plasmids containing the wild type and mutant cDNAs were linearized with XhoI and RNAs were transcribed and capped *in vitro* using the T7 RNA promoter (MEGAscript kit, Ambion). *X. laevis* oocytes were injected with 50 ng of cRNA encoding each protein. Oocytes were maintained at 18 °C in OR2 supplemented with penicillin (10,000 units/ml)/streptomycin (10 mg/ml) for 5–8 days before experiments.

Electrophysiology—Electrophysiology experiments were performed using a two-electrode voltage clamp with a rapid perfusion chamber. Oocytes were bathed in Na^+ solution composed of the following: 100 mM NaCl, 2 mM KCl, 1 mM $MgCl_2$, 1 mM $CaCl_2$, 10 mM Hepes/Tris, pH 7.4, and in Na^+-free solution, with choline chloride replacing NaCl. To measure sugar-induced current, the membrane potential was held at −50 mV and stepped for 100 ms from −150 mV to +50 mV or to +110 mV in 20-mV increments. The sugar-dependent current was defined as the difference between the current recorded in sugar and the previous record in Na^+ solution alone. Experiments were controlled, and data were acquired using pClamp software (Axon Instruments). Apparent Na^+ affinity ($K_{0.5}^{Na+}$) was calculated by recording currents in 150 mM αM-Glc and in progressively increasing Na^+ concentrations (0–100 mM). Apparent sugar affinity ($K_{0.5}$) was obtained in 100 mM Na^+ with increasing sugar concentrations (0–150 mM). The steady-state currents at each membrane potential were fit to the following equation: $I = I_{max}[S]^n/(K_{0.5}{}^n + [S]^n)$, where I_{max} is the maximal current, [S] is the substrate concentration, $K_{0.5}$ is the substrate concentration for one-half I_{max}, and n is the Hill coefficient. For fitting of sugar dose response curves, n was set to 1.

Presteady-state Currents—The "off" currents were fit with double exponentials, and the membrane capacitive component obtained from the fit was subtracted from the current record, leaving the currents attributable to the transporter. The presteady-state transient charge, Q, was determined by integration of this transient off current with time, and the distribution of the charge moved as a function of membrane voltage (V) was calculated by fitting the data with the Boltzmann equation: $(Q - Q_{hyp})/Q_{max} = 1/(1 + \exp(z(V - V_{0.5})F/RT))$, where $Q_{max} = Q_{dep} - Q_{hyp}$ (Q_{dep} and Q_{hyp} are Q at depolarizing and hyperpolarizing limits, respectively), F is Faraday's constant, R is the gas constant, and T is the absolute temperature. $V_{0.5}$ is the membrane potential where there is 50% charge transfer, and z is the apparent valence of movable charge. Fits of data with equations were performed using SigmaPlot (version 9.0).

Sugar Transport—Oocytes were incubated in 50 μM, 1 mM, or 6 mM of αM-Glc (as indicated in each experiment) with traces of [^{14}C]αM-Glc for 1 h in Na^+ solution or in Na^+-free solution. After the incubation, the oocytes were washed with cold Na^+-free solution and individually solubilized. Sugar uptake was determined by using a scintillation counter. Sugar uptake in noninjected oocytes from the same batch of oocytes was used as control.

Stoichiometry Experiments—Oocytes clamped at −90 mV were perfused with 5 mM αM-Glc with traces of radioactive αM-Glc. In each oocyte, the sugar-induced current was recorded during the incubation. After the incubation, the oocyte was removed from the chamber, washed, and solubilized, and radioactive sugar uptake was determined by scintillation counting. αM-Glc uptake into noninjected oocytes from the same batch was used to correct for background endogenous uptake. Sugar-induced current was obtained as the difference between baseline and αM-Glc-induced current and integrated over the time course of the experiment. Then, the current was converted to its molar equivalent by using Faraday's constant as described previously (11).

RESULTS

WT-mSGLT3b and the mutant proteins G457E and G457Q were expressed in oocytes to test for differences in their function. First, we tested whether glucose induced any current in the proteins. The oocytes were clamped at −50 mV and glucose-induced currents were recorded at different voltages, ranging from −150 to +50 mV. Fig. 2 shows examples of in-

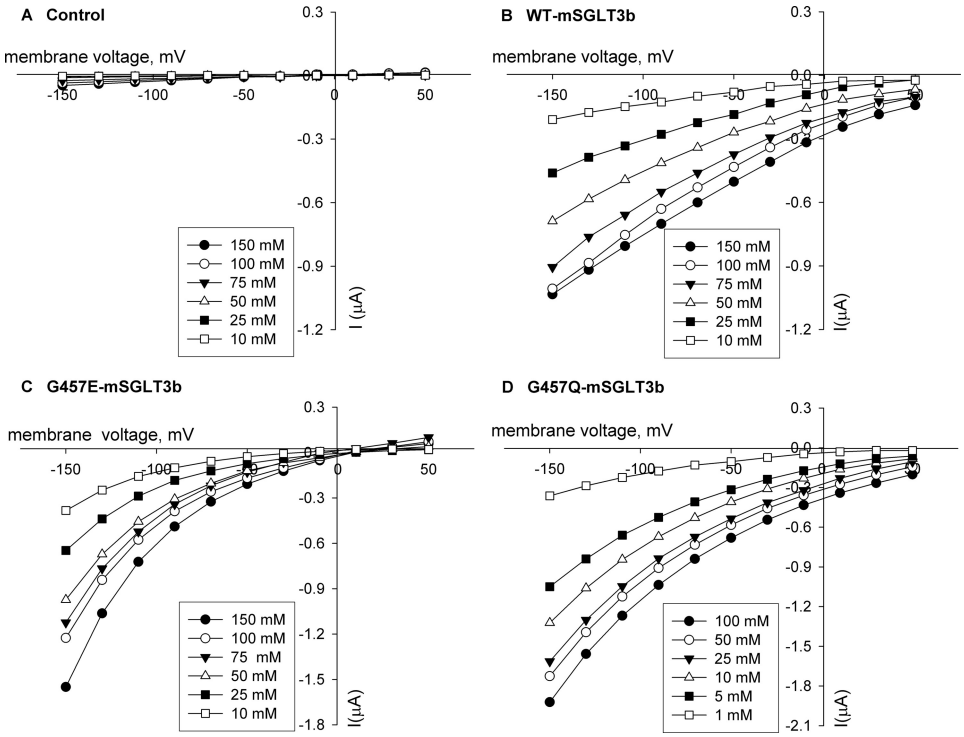

FIGURE 2. **Glucose-induced currents in a control oocyte and in WT-mSGLT3b-, G457E-, and G457Q-expressing oocytes.** Steady-state currents induced by various concentrations of glucose at voltages ranging from −150 to +50 mV were recorded from oocytes injected with RNA and expressing each of the constructs. Results from individual oocytes are shown.

duced currents recorded from WT-mSGLT3b (Fig. 2*B*), G457E (Fig. 2*C*), and G457Q (Fig. 2*D*) at those voltages, bathed in different glucose concentrations. The large currents that some of the glucose concentrations induced illustrate that there was robust expression of the three different clones in the oocytes. In addition, although the currents at any given sugar concentration through WT-mSGLT3b were approximately ohmic, there appeared to be increased voltage dependence in G457Q, and more dramatically in G457E, indicating that the nature of the residue at 457 affects the voltage dependence of the protein.

Because a mutation at amino acid 457 in human SGLT1 can lead to the disease glucose-galactose malabsorption due to the lack of sugar transport (7, 8), and the equivalent residue already present in the human SGLT3 appears to prevent glucose transport (3), we tested whether the mSGLT3b mutants have altered glucose transport properties. Fig. 3 shows that in the presence of 50 μM αM-Glc for 1 h, αM-Glc transport increased ~4-fold in G457Q (36 ± 5 pmol; $n = 4$) compared with WT-mSGLT3b (9 ± 0.2 pmol; $n = 4$) but was reduced to noninjected control levels (2.5 ± 0.2 pmol; $n = 4$) in G457E (2 ± 0.1 pmol; $n = 4$). Additionally, we found that sugar uptake in WT-mSGLT3b and G457Q was Na^+-dependent, as removal of Na^+ from the bath abolished uptake. These results indicate that in 50 μM αM-Glc, glutamine at residue 457 in mSGLT3b increases the sugar transport, whereas glutamate decreases sugar transport.

Apparent sugar affinities ($K_{0.5}$) were calculated for WT-mSGLT3b and for the mutants G457E and G457Q. Table 1 presents the means of the apparent affinities for glucose and αM-Glc measured at −90 mV. The apparent affinities

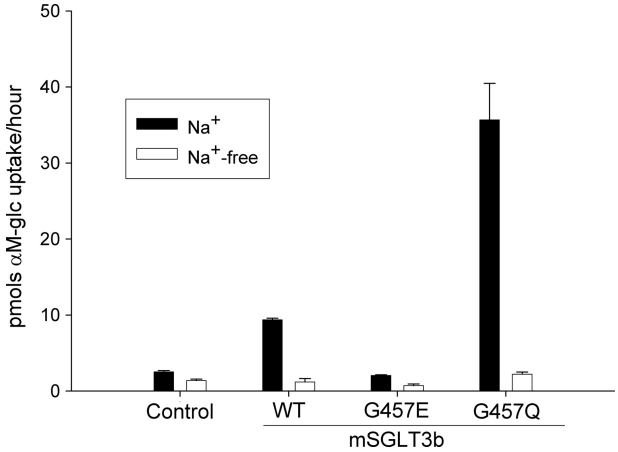

FIGURE 3. **Residue 457 affects sugar transport.** Sugar uptake in noninjected oocytes and those expressing WT-mSGLT3b, G457E, or G457Q in the presence or absence of Na^+. Oocytes expressing WT-mSGLT3b transport more sugar than control oocytes. The mutation G457E abolished sugar transport, whereas G457Q dramatically enhanced sugar transport in these experimental conditions (100 mM Na^+ and 50 μM αM-Glc). Data are mean ± S.E.

TABLE 1

Apparent affinities in mM for glucose and αM-Glc for WT-mSGLT3b, G457E, and G457Q, measured at −90 mV in oocytes

Values shown are mean ± S.E. and the number of experiments varies between two and six.

Sugar	WT-mSGLT3b	G457E	G457Q
Glucose	77 ± 3	59 ± 4	6 ± 0.2
αM-Glc	62 ± 5	65 ± 0.1	9 ± 0.6

of WT-mSGLT3b for αM-Glc and glucose were 62 ± 5 mM ($n = 5$) and 77 ± 3 mM ($n = 6$), respectively. These apparent sugar affinities are low compared with SGLT1 or

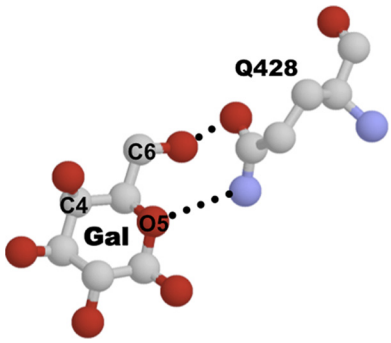

FIGURE 4. **Interaction between galactose (*Gal*) and residue Gln^{428} in vSGLT (5).** The figure shows amino acid Gln^{428}, which corresponds to Gly^{457} in mSGLT3b, interacting with the galactose molecule at hydroxyl group from C6 and the oxygen (O5) in the pyranose ring. Glucose differs from galactose only in the orientation of the hydroxyl group of the C4. *Red spheres* are oxygen molecules, *blue spheres* are nitrogen, and *dotted lines* represent hydrogen bonds.

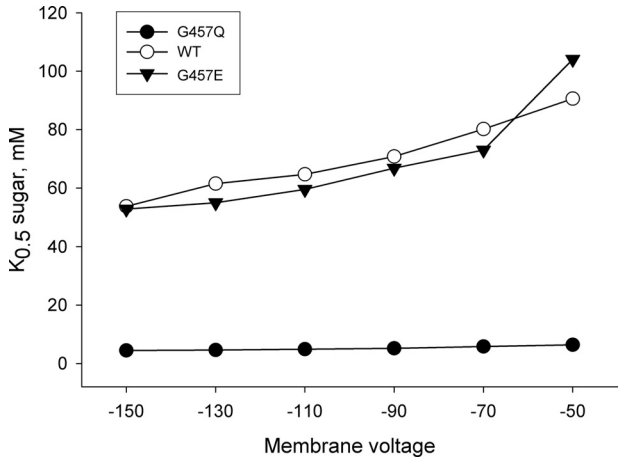

FIGURE 5. **Residue 457 has an effect on glucose affinity in mSGLT3b.** Glucose $K_{0.5}$ was calculated based on fits of equation (1) to sugar-induced currents in single oocytes expressing WT-mSGLT3b, G457Q, or G457E. Shown are $K_{0.5}$ values for glucose in WT-mSGLT3b and the mutants G457Q and G457E as a function of voltage. Note that the apparent affinities of WT-mSGLT3b and G457E are very similar. However, G457Q showed much higher apparent affinities. Average data from different oocytes at −90 mV are presented in Table 1.

SGLT2 but agree with the previously published mSGLT3b sugar affinities (12). G457E had very similar apparent sugar affinities to WT-mSGLT3b: $K_{0.5}$ for αM-Glc was 65 ± 0.1 mM (n = 2), and $K_{0.5}$ for glucose was 59 ± 4 mM (n = 4). However, when residue 457 was a glutamine, the apparent affinities were higher: 9 ± 0.6 mM (n = 4) and 6 ± 0.2 mM (n = 4) for αM-Glc and glucose, respectively. It was previously reported that the apparent affinity of WT-mSGLT3b for 6-deoxyglucose (6DO-Glc) is stronger than for glucose (12). Notably, we found here that the apparent affinity of G457Q for 6DO-Glc (4 ± 0.3 mM) was not significantly different than for glucose (Table 1). Thus, when residue 457 is glycine (WT) the −OH group of C6 of the pyranose ring prevents the sugar from binding strongly, but when it is glutamine (G457Q), the hydroxyl group does not affect the sugar binding, and glucose and 6DO-Glc interact strongly and similarly. This is interesting because the crystal structure of vSGLT shows that there is a direct interaction between the residue equivalent to the mammalian 457, Gln^{428} *in vibrio*, and the hydroxyl group of the C6 of the galactose (Fig. 4) (5). When the residue is short (glycine) the interaction is better when there is no −OH group at C6, and, when the residue is longer (glutamine) the interaction is not affected if there is no −OH group. Thus, the difference in apparent affinities between glucose and 6DO-Glc in mSGLT3b and G457Q could be due to allosteric alteration of the binding site, to differences in formation of hydrogen bonds, or both.

Fig. 5 shows the $K_{0.5}$ values for glucose at different voltages in individual oocytes expressing each of the three proteins, demonstrating that WT-mSGLT3b and G457E had the same apparent affinity at all the voltages tested, whereas G457Q resulted in stronger apparent affinity.

We next calculated the apparent Na^+ affinity, $K_{0.5}^{Na+}$, for G457Q and G457E. The $K_{0.5}^{Na+}$ for WT-mSGLT3b is ~ 20 mM (12). Although the residue analogous to 457 in vSGLT is known to interact directly with the sugar molecule (5), we found that mutations at this residue in mSGLT3b affected the apparent affinity for Na^+. Fig. 6*A* shows sugar-induced currents at different Na^+ concentrations from WT-mSGLT3b, G457Q, and G457E at −50 mV. The lowest apparent Na^+ affinity belonged to G457E and the highest to G457Q, whereas WT-mSGLT3b had an intermediate apparent affinity. We also calculated these apparent Na^+ affinities across a range of voltages (Fig. 6*B*) and found that the apparent affinity for G457Q ranged from 11 ± 2 mM at −150 mV to 21 ± 4 mM at −10 mV (data are the mean ± S.E. of four different experiments). Comparing these results with the WT-mSGLT3b apparent affinities (data from Ref. 12), the apparent affinity of Na^+ for G457Q is between two to three times higher than for WT-mSGLT3b. This change may be due to higher sugar affinity as $K_{0.5}^{Na+}$ is measured by sugar-induced currents at different [Na^+]. For G457E-mSGLT3b, it was not possible to calculate the $K_{0.5}^{Na+}$ at voltages between −150 and −70 mV because the currents did not saturate and could not be accurately fit to a Hill equation. The data obtained at more depolarizing voltages indicated that the $K_{0.5}^{Na+}$ values are higher than the $K_{0.5}^{Na+}$ obtained for the WT-mSGLT3b protein, and the $K_{0.5}^{Na+}$ values are even higher at hyperpolarizing voltages. Because the apparent sugar affinity was higher in G457Q than in WT-mSGLT3b, the differences shown in $K_{0.5}^{Na+}$ may be an indirect effect of the differences in sugar affinity. However, the apparent sugar affinities for WT-mSGLT3b and G457E were similar; thus, the differences observed between their $K_{0.5}^{Na+}$ values were not due to different sugar affinities.

Because the apparent affinities of sugar were higher for G457Q than for G457E and WT-mSGLT3b, we thought this might underlie the large difference we observed in the magnitude of sugar uptake between them (Fig. 3). Therefore, we repeated the sugar transport experiments at sugar concentrations that were ~10% of the $K_{0.5}$ of each of the respective proteins (Fig. 7). In these experiments, the external sugar concentrations were 6 mM for WT-mSGLT3b and G457E, and 1 mM for G457Q. At these concentrations, the sugar transport was similar in the WT-mSGLT3b and in G457Q-expressing oocytes. These data, compared with the data obtained with 50 μM sugar concentration, clearly show that apparent sugar af-

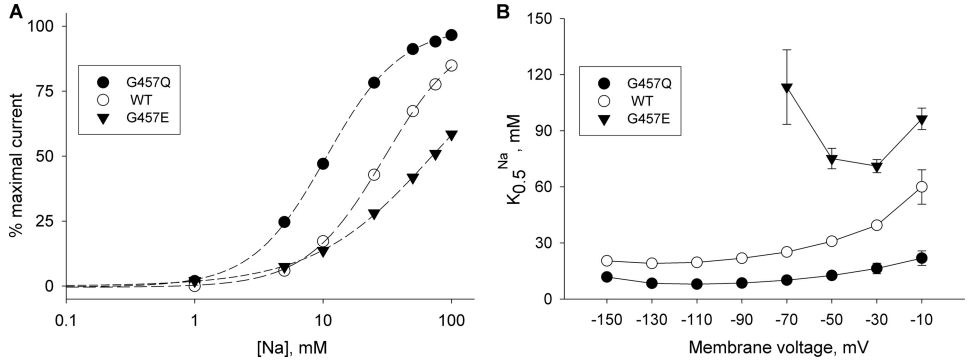

FIGURE 6. **Residue 457 influences the apparent Na^+ affinity.** *A*, apparent Na^+ affinities were measured in WT-mSGLT3b, G457Q, or G457E expressing oocytes at −50 mV. Raw currents at different [Na^+] were fit with the Hill equation (*dotted lines*). Data shown were normalized between the minimum and maximum as defined by the fit to display the shifts in $K_{0.5}^{Na+}$. For the individual experiments shown, $K_{0.5}^{Na+}$ in WT-mSGLT3b was 30 ± 1.3 mM, G457Q was 11 ± 0.2 mM, and G457E was 71 ± 11 mM. *B*, average $K_{0.5}^{Na+}$ from WT-mSGLT3b ($n = 4$), G457Q ($n = 4$), or G457E ($n = 4$). In G457E, we were only able to fit the data between −10 and −70 mV, and the data suggest that glutamate increases the $K_{0.5}^{Na+}$. Data shown are mean ± S.E.

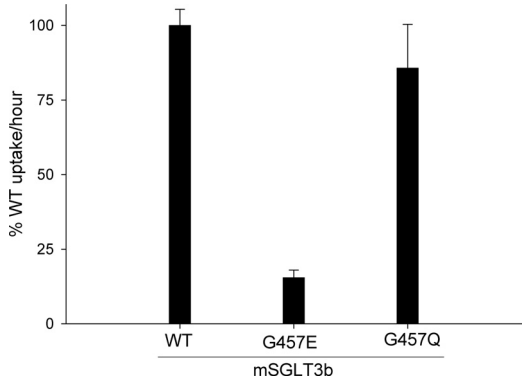

FIGURE 7. **Sugar transport is decreased in G457E.** Uptake of αM-Glc in WT-mSGLT3b, G457Q, and G457E as percentage of WT-mSGLT3b uptake. The concentration of sugar in the bath for each protein was adjusted to 10% of the $K_{0.5}$ for each respective protein (6 mM for WT and G457E, 1 mM for G457Q). The average sugar uptake of WT-mSGLT3b (1,243 pmol) was normalized to 100%. The uptake into comparably incubated noninjected oocytes has been subtracted in each case. Under these conditions, WT and G457Q showed very similar amounts of uptake, whereas G457E remained transport-deficient. Data shown are mean ± S.E. ($n = 10$).

finities account for the differences in amount of sugar uptake within these transporters when performing the experiment with low concentrations of the substrate (Fig. 3) in WT-mSGLT3b and G457Q. However, the transport for G457E was still low, only ~15% that of WT-mSGLT3b, indicating that G457E has less sugar transport capability.

The question remains as to why the sugar transport in G457E was so much lower than the WT-mSGLT3b. We therefore analyzed the mutant G457E in more depth.

We analyzed presteady-state currents of WT-mSGLT3b, G457Q, and G457E. Presteady-state currents represent partial reactions of the transport cycle that are voltage-dependent. By analyzing those currents, we obtained information on the distribution of the transporter in different states. Fig. 8*A* shows currents of one G457E-expressing oocyte in the presence of Na^+ and without sugar. The figure shows the currents of an oocyte clamped at −50 mV and when the voltage was jumped from −150 to +50 mV in +20-mV increments. WT-mSGLT3b, G457E, and G457Q presteady-state currents were analyzed to obtain the charge transfer (Q) at each voltage and to fit those data with a Boltzmann equation. Charge/voltage obtained for G457E is presented in Fig. 8*B* (*inverted triangle*). For comparison, we also plotted data from WT-mSGLT3b to show how G457E data were shifted to depolarizing voltages. The same Q/V plot and analysis were done with G457Q (data not shown). Data obtained from the fit to the Boltzmann equation (*dotted line*) in G457E and G457Q along with the data for WT-mSGLT3b (from Ref. 12) are presented in Table 2. $V_{0.5}$ in G457E was +36 mV, whereas in G457Q, it was +3 mV, and this shift in $V_{0.5}$ is even greater when we compare it with the $V_{0.5}$ of WT-mSGLT3b, −17 mV. These data indicate that at the same membrane potential, the three proteins have different distributions among the different states of the protein cycle.

Apart from the $V_{0.5}$, the other kinetic parameters obtained from analyzing the presteady-state currents were similar in the three proteins. Turnover numbers, calculated as I_{max} divided by Q_{max} (as previously described for other SGLT proteins (13)) were 76, 64, and 75 cycles per second in G457E, G457Q, and WT-mSGLT3b respectively, and the Q_{max} were 17, 25, and 25 nC. These Q_{max} values indicate that the transport levels are comparable and that decreased expression levels do not explain the lower sugar uptake in G457E.

Fig. 8*C* shows the average sugar-induced current in G457E and WT-mSGLT3b expressing oocytes (mean ± S.E.). At −150 mV, the sugar-induced current in G457E was the same as in WT-mSGLT3b. However, at more depolarizing voltages, the induced currents were lower in G457E than in the WT-mSGLT3b protein. These lower currents could explain, at least partially, why the sugar transport in G457E expressing oocytes is lower than in WT-mSGLT3b because the resting potential of the expressing oocytes is between −30 and −50 mV, and Fig. 7 represents sugar transport measured in nonclamped oocytes.

Finally, we tested the ratio of charge to sugar transport (Fig. 8*D*). SGLT1 transports two sodium ions with each sugar (14). The WT-mSGLT3b ratio was 2.6 charges per sugar molecule (data from Ref. 12), showing that this transport was not as tightly coupled as in SGLT1. In G457E, we found that charge: sugar transport was even more uncoupled, with an average of 4.5 charges per sugar molecule. Thus, the same magnitude of sugar-induced current in G457E as in WT-mSGLT3b will

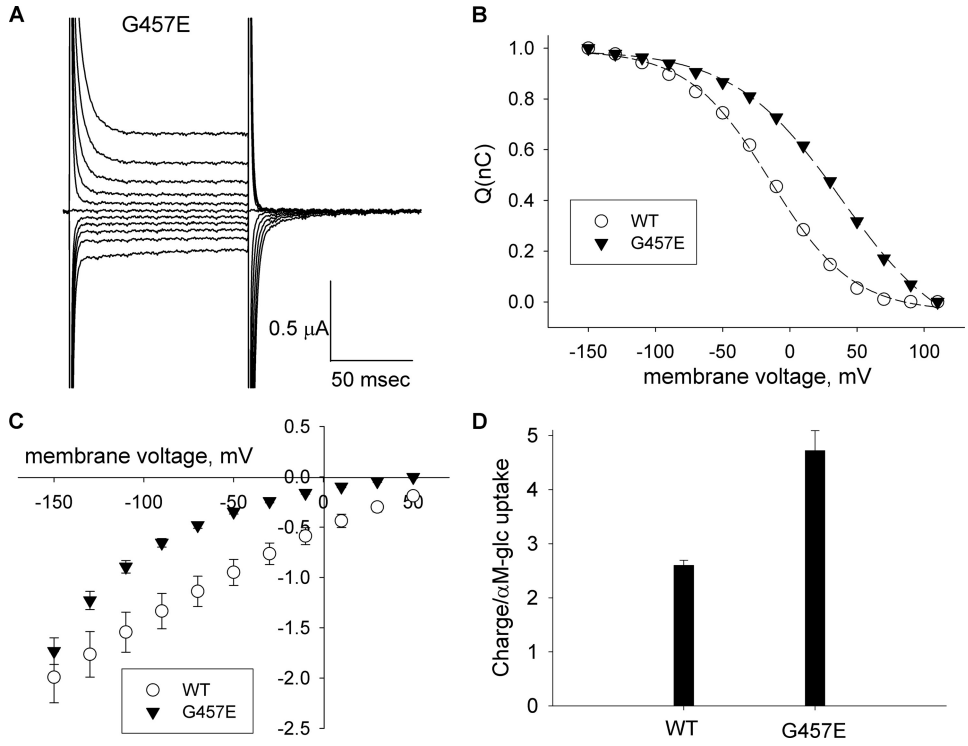

FIGURE 8. **Voltage dependence and stoichiometry of G457E.** *A*, currents were recorded in the absence of sugar from oocytes expressing G457E, held at −50 mV and subjected to 100-ms test pulses from −150 to + 50 mV. *B*, charge movement, Q, in G457E was found by integrating the noncapacitive presteady-state component of the off currents. $V_{0.5}$ was depolarized compared with $V_{0.5}$ for WT-mSGLT3b, suggesting that at rest, the Na^+- and sugar-binding sites are more likely to be facing outward. *C*, average sugar-induced currents of WT-mSGLT3b ($n = 6$) and G457E ($n = 7$) as a function of voltage. *D*, stoichiometry of charge movement to sugar uptake, measured by simultaneously recording currents and sugar uptake under voltage clamp. G457E was significantly uncoupled compared with WT-mSGLT3b (12), which is itself slightly uncoupled compared with SGLT1 (2:1, Ref. 14). Data shown in *C* and *D* are mean ± S.E.

TABLE 2

Summary of kinetic parameters

Shown are the parameters obtained from analyzing presteady-state currents on G457Q and G457E. The table includes values for WT-mSGLT3b from Ref. 12. These data were derived from fits of the Boltzmann equation to *Q*/*V* distributions as shown in Fig. 8. Q_{max} is the total charge movement by the protein. $V_{0.5}$ is the voltage at which the charge is equally distributed between inward and outward facing conformations, and turnover is the rate at which the protein cycles. All parameters, except $V_{0.5}$, were similar between both mutants and similar to WT-mSGLT3b. $V_{0.5}$ in G457E is more depolarized than in G457Q. Data are shown as mean ± S.E. ($n = 6–8$).

	WT-mSGLT3b	G457E	G457Q
I_{max} (nA)	1800 ± 250	1200 ± 130	1600 ± 330
Q_{max} (nC)	25 ± 4	17 ± 2	25 ± 4
$V_{0.5}$ (mV)	−17 ± 1	36 ± 2	3.3 ± 4
Turnover (cycles sec^{-1})	75 ± 3.4	76 ± 8	64 ± 6

correspond with less sugar transported by G457E compared with WT-mSGLT3b. Thus, the lower rate of sugar transport observed in G457E (Fig. 7) can be due to either the decreased sugar-induced currents at resting potentials (Figs. 2 and 8*C*), to the uncoupled charge:sugar transport phenotype (Fig. 8*D*), or to a combination of both.

DISCUSSION

The goal of this work was to understand the functional differences between SGLT1 and SGLT3. The advantage of studying mSGLT3b instead of human SGLT3 is that we can analyze presteady-state currents and calculate the apparent affinities of Na^+. Typical recordings of hSGLT3 do not show presteady-state currents (3) and, to date, the apparent Na^+ affinity in hSGLT3 has not been resolved. We studied the mSGLT3b mutants G457E and G457Q, which recapitulate the amino acids at residue 457 in hSGLT3 and SGLT1, respectively. Thus, we investigated the modifications in apparent sugar and Na^+ affinities, ability to transport sugar, the distribution of the protein in different states, and the charge-to-sugar stoichiometry to suggest a mechanistic model for current transport uncoupled from sugar transport.

Apparent Na^+ Affinity—We found that G457E has lower apparent Na^+ affinity than WT-mSGLT3b, whereas both have the same apparent sugar affinity. Can a different distribution of G457E between inward and outward facing states explain this lower Na^+ affinity? A simplified six-state ordered kinetic model that described the states of SGLT1 was proposed earlier (15, 16). Half of the states have the binding site of the protein facing the extracellular space (C1, C2, and C3 of Fig. 9) and half the intracellular space (C4, C5, and C6). By introducing glutamate at residue 457, we added an extra negative charge to an already voltage-dependent protein. Analyzing the presteady-state currents in G457E, we observed that the $V_{0.5}$, the voltage at which the charge is equally distributed between inward and outward facing conformations, is more positive than in the WT-mSGLT3b protein (Fig. 8, *A* and *B*, and Table 2). This means that at physiological voltages a higher percentage of the protein will be facing out. The extra negative charge in the protein weakens the apparent affinity for Na^+ while leaving the apparent sugar affinity unaffected. Hence, the favorable distribution of G457E toward the outward facing conformation compared with WT-mSGLT3b

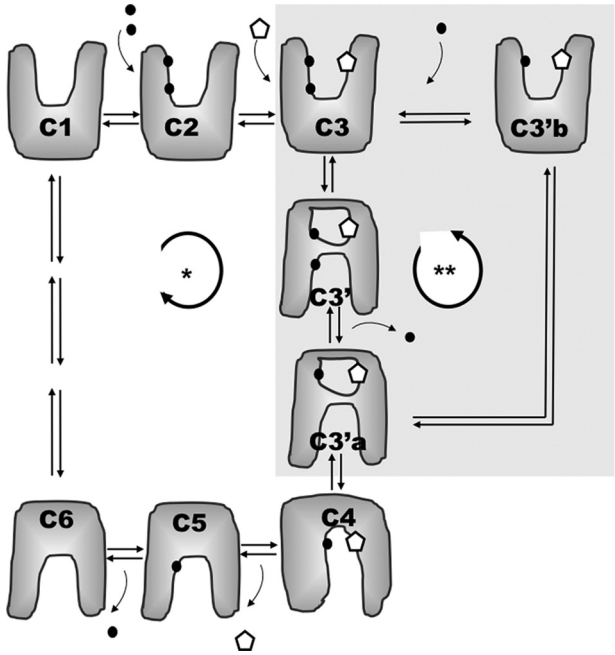

FIGURE 9. **Intermediate conformational states in the transport cycle of SGLT proteins.** Cartoon adapted from the transport model previously described for SGLT proteins (modified from Ref. 15) that includes intermediate states between C3 and C4. Intermediate states between C6 and C1 earlier described are represented as *multiple arrows* joining C6 and C1 (19). The simplified kinetic model suggests that the empty protein facing the outside of the cell (C1) binds first two Na^+ (C2) and then sugar (C3). Then, the protein reaches an intermediate state where one Na^+ is exposed (C3′) and then released (C3′a), whereas the other Na^+ and the sugar are occluded. An additional conformational change exposes the sugar and Na^+ (C4), and they are then released (C5 and C6). The empty transporter (C6) faces again the extracellular compartment (C1). From the state where the first Na^+ is released, C3′a, if the sequence of the protein does not allow the next conformational change that exposes the other Na^+ and sugar (C4), the protein will go into conformation C3′b, facing outward again. Protein will be back in conformation C3 if one Na^+ is bound. This alternate cycle (**) will result with Na^+ transport with no sugar transport. Thus, in SGLT1s, the protein will tend to follow the cycle (*). However, if the ratio of charge to sugar transport is >2:1, in addition to cycle (*), a percentage of the protein will follow cycle (**), which we call a sugar-dependent ion leak. *Circles* represent Na^+ ions and pentagon the sugar.

does not explain the weaker $K_{0.5}^{Na+}$ of the protein because that distribution would cause a stronger affinity.

The introduction of a negative charge at 457 weakened the apparent affinity of Na^+, whereas a neutral mutation (G457Q-mSGLT3b) significantly strengthened it (although this could be due to a higher glucose affinity in G457Q). In vSGLT, one Na^+-binding site was proposed to be ~8–10 Å from the bound sugar based on structural homology to LeuT. This would correspond with the Na2 site in LeuT. In vSGLT, the Na1 site was not detected, but in LeuT, the octahedral coordination for that Na1 includes one leucine carboxyl oxygen (4, 5, 9). We found that glutamate at residue 457 lowered the apparent Na^+ affinity. This suggests that mutations at 457 may change the geometry of a nearby Na^+ binding site, Na2, but that residue 457 is not part of the Na^+ binding site. However, we cannot rule the possibility that in SGLT3b one Na^+ binds to the sugar, similarly to Na1 in LeuT, so that alteration of the sugar binding will directly affect that Na^+ binding.

Uncoupled Current to Sugar Transport—According to the existing six-state kinetic model developed for SGLT1 (16, 17), empty outward facing proteins (C1) first bind two sodium ions (C2), then bind one sugar molecule (C3) and undergo a subsequent conformational change that transitions the protein from outward to inward facing (C4) where the ligands are released (C5 and C6) before returning to the outward facing empty conformation (C1). Among SGLT clones that transport with stoichiometries close to 2:1, all bind Na^+ with apparent affinities in the 10–30 mM range (SGLT1 (14), mSGLT3b (12), and pig SGLT3 (11)). In contrast, G457E had weaker Na^+ affinity and an uncoupled stoichiometry 4.5:1 (Fig. 8*D*), whereas the apparent affinity of human SGLT3 for Na^+ remains undetermined. Applying the six-state model to all SGLT proteins, one simple explanation for progressively more uncoupled stoichiometries is a greater fraction of proteins that undergo the C2–C5 transition, thereby releasing internal Na^+, but without any sugar binding or transport. However, this explanation cannot account for uncoupled current in its entirety. In particular, in human SGLT3, the current is sugar dependent yet none of the protein appears to reach state C4. What then is the determinant of sugar transport or nontransport in SGLT proteins?

The apparent affinity of sugar does not appear to determine sugar transport, as WT-mSGLT3b and G457Q transport equally well when the sugar concentration was normalized to their respective $K_{0.5}$ values (Fig. 7). However, G457E, with the same apparent sugar affinity but lower Na^+ affinity than WT-mSGLT3b, transports sugar less efficiently (Fig. 7) and more uncoupled from the charge transport (Fig. 8*D*). These data suggest that the ability or failure to transport sugar depends upon completion of the conformational change after sugar binding. In other transporters, the existence of intermediate states between C3 to C4 has been proposed (18). In SGLT1, although intermediate states have been described between C6 and C1 (19), none has been proposed between C3 and C4.

Intermediate Conformational States—The order of release of Na^+ and sugar by SGLT is not yet well established. Equilibrium simulations performed in vSGLT suggest that Na^+ is released intracellularly very quickly and before the sugar (20). Moreover, using molecular dynamics simulations in LeuT, it was proposed that one Na^+ is released before the other Na^+ and the substrate (21). Thus, in our proposed model for SGLT (Fig. 9), one Na^+ is first released inside from an intermediate state (C3′) between C3 and C4, whereas sugar and the other Na^+ are occluded. Then, there is a conformational change that exposes the occluded Na^+ and sugar (C4) followed by their release (C5 and C6). Uncoupled stoichiometries could be explained by the transition from C3′ to C3′a, where the first Na^+ is released but the conformational change to expose Na^+ and sugar does not occur. The side chain at residue 457 may be responsible for preventing the progression (C3′a to C4) toward the conformation that favors intracellular release of the other Na^+ and sugar; thus, the transporter goes back toward the outward-facing conformation (C3′a to C3′b to C3). In fact, it was recently proposed that charge and polarity of residue 457 affect the conformational changes that occur after Na^+ and sugar binding (22). Human SGLT3, which

transports ions but not sugar, would then be the most extreme manifestation of this failure to complete the translocation step, shifting the protein toward C3′a and with no protein completing the C3′a to C4 transition.

An alternative explanation for the failure to complete C3′a to C4 transition could be due to the premature release of the Na^+ when apparent Na^+ affinity is low. In addition, our data do not differentiate whether only one or both Na^+ ions are released during sugar-dependent ion leak.

In conclusion, the nature of the side chain at amino acid 457 has an effect on the apparent sugar and Na^+ affinities and, moreover, on the uncoupled charge transport. Sugar affinity is likely to be affected by a direct effect of the sugar binding site, but the Na^+ affinity may be affected by allosterically altering the Na^+ binding site. Uncoupled stoichiometries may reflect the existence of an intermediate state from which the protein can release one Na^+. This must be followed by difficulties in progressing to states where the other Na^+ and sugar can be released. The degree of uncoupling in transport would then be dependent on the energetic balance between transition to the fully inward facing state, where the other Na^+ and sugar could be released, *versus* returning to an outward facing conformation.

Acknowledgments—We thank H. P. Larsson and B. A. Hirayama for insightful comments on the paper.

Addendum—After initial review, an additional structure of vSGLT was released by Watanabe *et al.* (23) who independently proposed intracellular Na^+ release from an intermediate state consistent with our results and proposed model.

REFERENCES

1. Wright, E. M., and Turk, E. (2004) *Pflugers Arch.* **447,** 510–518
2. Diez-Sampedro, A., Hirayama, B. A., Osswald, C., Gorboulev, V., Baumgarten, K., Volk, C., Wright, E. M., and Koepsell, H. (2003) *Proc. Natl. Acad. Sci. U.S.A.* **100,** 11753–11758
3. Bianchi, L., and Díez-Sampedro, A. (2010) *PLoS One* **5,** e10241
4. Abramson, J., and Wright, E. M. (2009) *Curr. Opin. Struct. Biol.* **19,** 425–432
5. Faham, S., Watanabe, A., Besserer, G. M., Cascio, D., Specht, A., Hirayama, B. A., Wright, E. M., and Abramson, J. (2008) *Science* **321,** 810–814
6. Díez-Sampedro, A., Wright, E. M., and Hirayama, B. A. (2001) *J. Biol. Chem.* **276,** 49188–49194
7. Wright, E. M., Turk, E., and Martin, M. G. (2002) *Cell Biochem. Biophys.* **36,** 115–121
8. Lam, J. T., Martín, M. G., Turk, E., Hirayama, B. A., Bosshard, N. U., Steinmann, B., and Wright, E. M. (1999) *Biochim. Biophys. Acta* **1453,** 297–303
9. Yamashita, A., Singh, S. K., Kawate, T., Jin, Y., and Gouaux, E. (2005) *Nature* **437,** 215–223
10. Voss, A. A., Díez-Sampedro, A., Hirayama, B. A., Loo, D. D., and Wright, E. M. (2007) *Mol. Pharmacol.* **71,** 628–634
11. Díez-Sampedro, A., Eskandari, S., Wright, E. M., and Hirayama, B. A. (2001) *Am. J. Physiol. Renal Physiol.* **280,** F278–282
12. Aljure, O., and Díez-Sampedro, A. (2010) *Am. J. Physiol. Cell. Physiol.* **299,** C58–65
13. Panayotova-Heiermann, M., Loo, D. D., Lostao, M. P., and Wright, E. M. (1994) *J. Biol. Chem.* **269,** 21016–21020
14. Mackenzie, B., Loo, D. D., and Wright, E. M. (1998) *J. Membr. Biol.* **162,** 101–106
15. Parent, L., Supplisson, S., Loo, D. D., and Wright, E. M. (1992) *J. Membr. Biol.* **125,** 63–79
16. Loo, D. D., Hazama, A., Supplisson, S., Turk, E., and Wright, E. M. (1993) *Proc. Natl. Acad. Sci. U.S.A.* **90,** 5767–5771
17. Loo, D. D., Hirayama, B. A., Gallardo, E. M., Lam, J. T., Turk, E., and Wright, E. M. (1998) *Proc. Natl. Acad. Sci. U.S.A.* **95,** 7789–7794
18. Forrest, L. R., and Rudnick, G. (2009) *Physiology* **24,** 377–386
19. Loo, D. D., Hirayama, B. A., Karakossian, M. H., Meinild, A. K., and Wright, E. M. (2006) *J. Gen. Physiol.* **128,** 701–720
20. Li, J., and Tajkhorshid, E. (2009) *Biophys. J.* **97,** L29–31
21. Shi, L., Quick, M., Zhao, Y., Weinstein, H., and Javitch, J. A. (2008) *Mol. Cell* **30,** 667–677
22. Liu, T., Krofchick, D., and Silverman, M. (2009) *Biophys. J.* **96,** 748–760
23. Watanabe, A., Choe, S., Chaptal, V., Rosenberg, J. M., Wright, E. M., Grabe, M., and Abramson, J. (2010) *Nature* **468,** 988–991